A New Adaptive Imaging Technique Using Optimal Aperture Size

Meng-Lin Li and Pai-Chi Li
Department of Electrical Engineering, National Taiwan University,
Taipei, Taiwan, R. O. C.

Abstract - Focusing errors caused by sound-velocity inhomogeneities in human tissue, also known as phase aberrations, reduce coherence of the received signals. Low coherence results in high sidelobes in the radiation pattern and degrades contrast resolution. This paper proposes an efficient adaptive imaging technique using optimal receive aperture size. The technique determines the optimal aperture size based on the coherence factor, which quantifies coherence of the received array signals and a threshold can be set to distinguish a mainlobe signal from sidelobes. With the thresholding, the receive aperture size at each imaging position can be optimally determined so as to enhance the mainlobe signal and suppress the sidelobes. Thus, focusing errors can be reduced. Efficacy of the proposed technique was demonstrated by experimental array data. This technique effectively reduces sidelobes and decreases speckle variance. The characteristics of the proposed technique are also explored.

I. INTRODUCTION

Focusing errors caused by sound-velocity inhomogeneities in human tissue, also known as phase aberrations, reduce coherence of the received signals. Low coherence results in high sidelobes in the radiation pattern and degrades contrast resolution. Several adaptive imaging techniques have been proposed in the past to compensate for such errors. Among them, the correlation based techniques have been widely adopted, but its performance is primarily limited by the elevational aberrator integration error of a one-dimensional array[1]. Another approach is based on adaptive removal of undesired sidelobe contributions utilizing multiple receive beams[2]. Although this approach does not require elevational sampling of the aperture, its computation requirements prohibit its real-time implementation.

In this paper, an efficient adaptive imaging technique using optimal receive aperture size is proposed. The technique determines the optimal aperture size based on the coherence factor (CF), which is defined as the ratio of the coherent energy to the incoherent energy. The coherence factor quantifies coherence of the received array signals, and a threshold can be set to distinguish a mainlobe signal from sidelobes. With the thresholding, the receive aperture size at each imaging position can be optimally determined so that the final array sum is maximum for the mainlobe and minimal for the sidelobe. Consequently, focusing errors can be reduced and image quality degradation resulting from undesired sidelobe contributions can be compensated. Measured ultrasound data are used to evaluate the efficacy of the adaptive receive aperture technique (ARAT) for diffuse scatterers. The proposed technique is also compared with the parallel adaptive receive compensation algorithm. Effects of the signal-to-noise ratio are also discussed.

II. COHERENCE FACTOR THRESHOLDING

The CF is defined as the ratio of the energy of the coherent sum obtain in a conventional delay-and-sum based beamformer to the total incoherent energy:

$$\mathrm{CF}(t) = \frac{\left|\sum_{i=0}^{N-1} C(i,t)\right|^2}{N\sum_{i=0}^{N-1}\left|C(i,t)\right|^2}, \qquad (1)$$

where t is the time index, N is the number of array channels used for beam formation, and $C(i,t)$ is the received signal of channel i after the correct receive delays have been applied[3]. The CF quantifies coherence of the received array signals.

Simulations were used to explore characteristics of the CF for signals coming from the mainlobe and the sidelobes. The simulated phased array had 64 elements with a center frequency of 3.5 MHz and a half-wavelength pitch. The transmit focal depth was 30 mm, and dynamic focusing was applied on receive. Only a near-field phase screen was simulated for all aberration cases, and the aberration profile was applied on both transmit and receive. Note that the images shown in all subsequent figures are sector-scan images

obtained prior to scan conversion.

Figs. 1(a)–(c) show the simulated 50-dB images of a point target at the transmit focal depth with maximum phase errors of 0, $\pi/4$, and $\pi/2$, respectively, at the imaging frequency of 3.5 MHz. The beam quality degrades as the maximum phase error increases. Fig. 1(d) shows the CFs at four imaging locations: the curves labeled A, B, C, and D correspond to the four image locations indicated by the four crosses in Figs. 1(a)–(c). With a larger maximum phase error, the CF decreases when the imaging position is located at the mainlobe (i.e., A). Note that the CFs of the imaging points located at the sidelobes (i.e., B, C, and D) are barely distinguishable from one another. They are much smaller than that at the mainlobe. Fig. 1(d) suggests that a threshold of CF may be set to distinguish a mainlobe signal from sidelobes.

To further study if the characteristics of the CF evident in Fig. 1(d) also exist for targets with diffuse scatterers, images of an anechoic cyst in a speckle-generating background were simulated. The cyst was centered at the transmit focal depth. Note that signals in the anechoic-cyst region are from unwanted sidelobe contribution; thus the CF values in the anechoic cyst region can be viewed as the CFs of the imaging points at the sidelobes. Fig. 2(a) shows mean values of the CF as a function of the maximum phase error. The solid and dashed lines show the mean values of the CF in the speckle and anechoic-cyst regions (i.e., sidelobes), respectively. The error bars indicate plus and minus one standard deviation relative to the mean value. The figure shows that the mean values of the CF in the speckle region are differentiable from those in the anechoic cyst. However, the standard deviations of the CFs in the speckle region are significantly larger than those in the cyst region. Such variations in the CF in the speckle region indicate that the CF also suffers from speckle noise. Such a large standard deviation (especially for the case with the $\pi/2$ maximum phase error) may lead to a significant error if a threshold of the CF is used to distinguish the speckle and anechoic-cyst (sidelobe contribution) signals.

Spatial low-pass filtering of the CF can reduce the CF variations in the speckle region, and thus may improve the ability to make this differentiation. Fig. 2(b) shows the corresponding results of the low-pass-filtered CF (LPF{CF}) in the same format as that in Fig. 2(a). To smooth out the standard deviations of the CF and to retain the mean values of the CF simultaneously, a simple two-dimensional moving-average low-pass filter is employed. The number of sample points corresponding to the –20 dB point spread function in azimuth times that in range is chosen as the kernel size of the low-pass filter. Such a filter size renders the two curves in Fig. 2(b), which are separable even for a maximum phase error of $\pi/2$. This figure shows that thresholding LPF{CF} allows signals from the speckle and anechoic-cyst (sidelobe contribution) regions to be differentiated, which is the basis of the proposed ARAT and is referred to as "CF thresholding" in this paper.

III. ADAPTIVE RECEIVE APERTURE TECHNIQUE

Section II demonstrates that CF thresholding can be used to distinguish speckle signals from the incoherent noise (i.e., sidelobe contribution). In addition, when phase aberrations are present, beam formation with a smaller receive aperture can result in a larger beam sum. An adaptive receive-aperture technique can be developed based on these two properties. Once the signals from the sidelobes (or the anechoic region) and the mainlobe (or the speckle region) are identified, the optimum number of receive channels at each imaging point, $N_{\text{optimal}}(t)$, can be adaptively determined as follows:

$$\begin{cases} N_{\text{optimal}}(t) = \{N \mid \max(S(N,t), N = N_{\min}, N_{\min}+1, \ldots, N_{\max}\}, \\ \qquad \text{if LPF}\{\text{CF}(t)\} \geq \text{CF}_{\text{threshold}} \\ N_{\text{optimal}}(t) = \{N \mid \min(S(N,t), N = N_{\min}, N_{\min}+1, \ldots, N_{\max}\}, \\ \qquad \text{if LPF}\{\text{CF}(t)\} < \text{CF}_{\text{threshold}} \end{cases}$$

, (2)

where $N_{\max}$ is the number of total active channels on receive, $N_{\min}$ is the lower bound of N_{optimal} that is used to avoid degradation of spatial resolution and to preserve the SNR, and N is the number of center receive channels used for the beam sum, $S(N,t)$, and ranges from $N_{\min}$ to $N_{\max}$. $\text{CF}_{\text{threshold}}$ is used to determine the location of the imaging point. When LPF{CF(t)} is smaller than $\text{CF}_{\text{threshold}}$, the imaging point is considered to be in the anechoic region (i.e., at the sidelobes); thus $N_{\text{optimal}}(t)$ should minimize $S(N,t)$ so that the signals coming from the sidelobes or the anechoic region can be suppressed. Otherwise, $N_{\text{optimal}}(t)$ should maximize $S(N,t)$ to enhance the signals from the mainlobe or the speckle region. Therefore, the degradation in image quality resulting from sound-velocity inhomogeneities can be reduced. The computational complexity of this technique is relatively low, and no iteration is needed.

IV. EXPERIMENTAL RESULTS

Three complete RF data sets with three levels of distortion were used to test the efficacy of the proposed ARAT. The data were acquired using a 64-element, 3.33-MHz phased-array transducer at a sampling frequency of 17.76 MHz. Dynamic receive focusing with an f/number of 2 was applied. Note that dynamic transmit focusing with the same f/number was also applied in order to test the proposed technique in the absence of influence from the transmit focal depth.

Fig. 3(a) shows the 60-dB image without distortion, and Figs. 3(b) and (c) show images of the phantom with 1× and 2× distortion, corresponding to maximum phase errors of π and 2π, respectively, at the imaging frequency of 3.33 MHz. Fig. 4 shows mean values of the LPF{CF} as a function of the maximum phase error for the experimental data, in the same format as that of Fig. 2. The upper and lower boxes in Fig. 3(a) indicate the speckle and anechoic-cyst regions, respectively, used for CF estimation in Fig. 4. From Fig. 4, experimental signals from the speckle region and from the anechoic cyst can be differentiated by CF thresholding, with $CF_{threshold}$ set at 0.05. Figs. 3(d)–(f) show the images of Figure 3(a)–(c), respectively, corrected using the ARAT. The figure demonstrates that the proposed technique noticeably improves the image quality in all cases. The improvement in image quality is evaluated using the standard deviation of the image intensity, in dB, in the speckle background and two indices related to contrast resolution: (i) the contrast ratio (CR), which is defined as the difference of the mean intensity in the background to the mean intensity in the cyst region, in dB, and (ii) the contrast-to-noise ratio (CNR), which is defined as the CR divided by the standard deviation of the image intensity in the background region. Figs. 5(a)–(c) shows the estimated standard deviation in the speckle background and the CR and CNR values for the images shown in Fig. 3. The lines with squares are the original values, and the lines with circles are the values corrected using the ARAT. The ARAT reduces the speckle variance in the speckle background and increases the CR and CNR in all cases.

V. DISCUSSION

The CF in (1) is defined without taking noise into consideration. The estimated CF is affected by noise, which in turn affects the accuracy of CF thresholding in the ARAT. The relationship between CF without noise and the estimated CF with a finite SNR (denoted by CF') can be expressed as follows [4]:

$$CF' = \frac{CF \cdot SNR + \frac{1}{N}}{1 + SNR}. \qquad (3)$$

Equation (3) shows that although the CF' is dependent on the SNR, the real CF that needs to be used for CF thresholding can still be retrieved once the SNR is estimated.

The contrast improvement of the ARAT was also compared with that of PARCA2 [2], using the same experimental data in Fig. 4. Three iterations were used for PARCA2. Figs. 3(g)–(i) show the PARCA2-corrected versions of the images in Figs. 3(a)–(c), respectively. The corresponding standard deviation in the speckle background and the CR and CNR values are included in Figs. 5 as lines with triangles. PARCA2 increases the speckle variance, as demonstrated in Fig. 3(h) and (i). With PARCA2, the standard deviation in the background region is significantly higher than that without correction as the maximum phase error increases. Hence, PARCA2 deteriorates the CNR of the corrected image with 2× distortion, as shown in Fig. 5(c). Note that applying the proposed ARAT reduces the standard deviation in the speckle background in all cases. In general, the CNR is higher when applying the proposed technique than that with PARCA2.

VI. CONCLUSIONS

This paper proposes an adaptive receive-aperture technique based on CF thresholding to reduce focusing errors caused by sound-velocity inhomogeneities in ultrasound imaging. The experimental results demonstrate the effectiveness of the proposed ARAT. The speckle variance was also reduced by the proposed technique. In addition, the performance of the ARAT can be further enhanced if the value of $CF_{threshold}$ can be optimized for different levels of phase aberration.

REFERENCES

[1] S. W. Flax and M. O'Donnell, "Phase-aberration correction using signals from point reflectors and diffuse scatterers: basic principles," *IEEE Trans. Ultrason., Ferroelect., Freq. Contr.*, vol. 35, no. 6, pp. 758–767, 1988.

[2] S. Krishnan, K. W. Rigby, and M. O'Donnell, "Efficient parallel adaptive aberration correction," *IEEE Trans. Ultrason., Ferroelect., Freq. Contr.,* vol. 43, no. 1, pp. 691–703, 1998.

[3] K. W. Hollman, K. W. Rigby, and M.

O'Donnell, "Coherence factor of speckle from a multi-row probe," in *Proc. IEEE Ultrason. Symp.*, 1999, pp. 1257–1260.
[4] P.-C. Li and M.-L. Li, "Adaptive imaging using the generalized coherence factor," *IEEE Trans. Ultrason., Ferroelect., Freq. Contr*, vol. 50, no. 2, pp. 128–141, 2003.

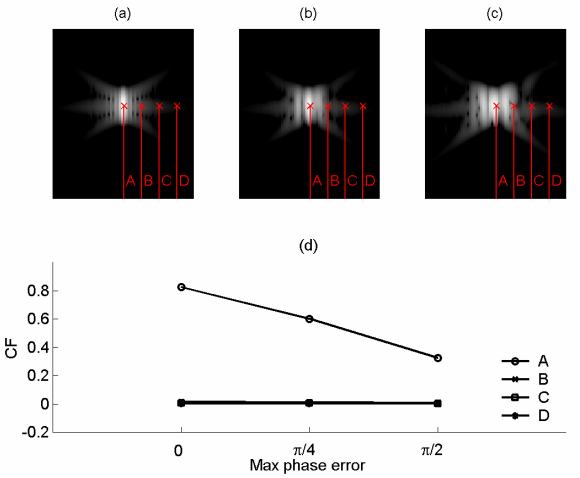

Fig. 1 (a)–(c) Simulated images of a point target at the transmit focal depth, with maximum phase errors. (d) The corresponding CFs at the imaging points indicated by the four crosses – A, B, C, D in (a)–(c).

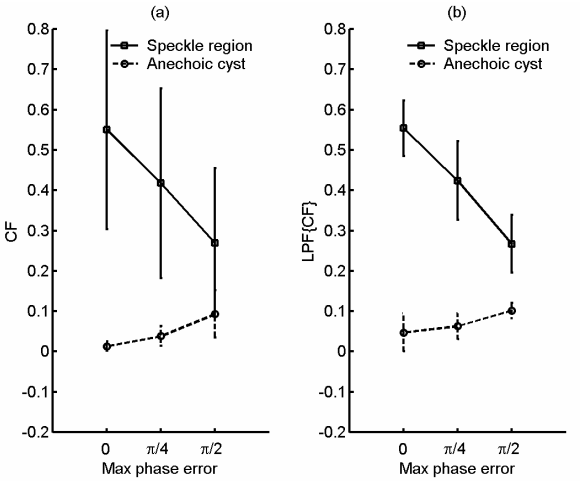

Fig. 2 Mean values of the original CF (a) and the corresponding LPF{CF} (b) as a function of maximum phase error for the simulated cyst images.

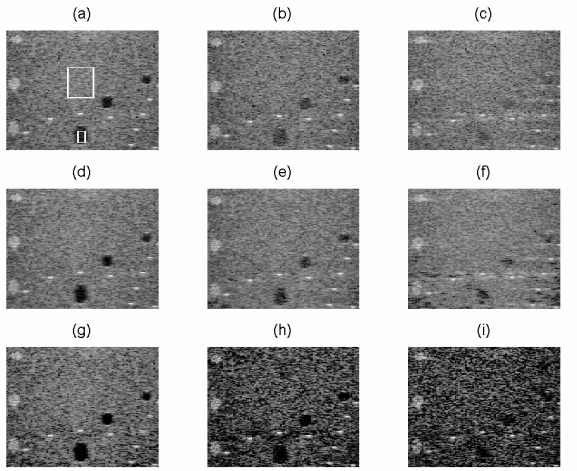

Fig. 3 Images of a tissue-mimicking phantom displayed over a 60-dB dynamic range. The top row shows the original images, the middle row shows the images obtained with the ARAT, and the bottom row shows the PARCA2-corrected images. (a), (d), (g) No distortion; (b), (e), (h) 1× distortion; and (c), (f), (i) 2× distortion.

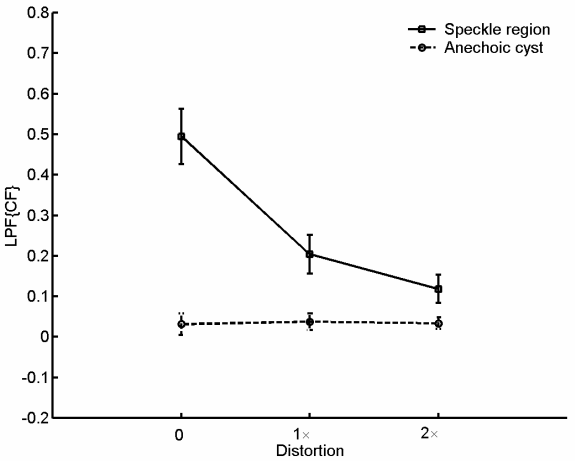

Fig. 4 Mean values of LPF{CF} as a function of maximum phase error for the experimental data.

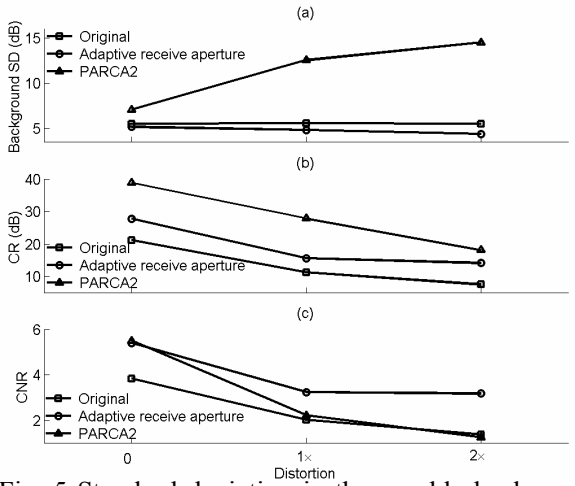

Fig. 5 Standard deviation in the speckle background (a) and the CR (b) and CNR (c) of the images of a tissue-mimicking phantom for different maximum phase errors.